Remote Sensing of Environment 271 (2022) 112907

Contents lists available at ScienceDirect

Remote Sensing of Environment

journal homepage: www.elsevier.com/locate/rse

Monitoring standing herbaceous biomass and thresholds in semiarid rangelands from harmonized Landsat 8 and Sentinel-2 imagery to support within-season adaptive management

Sean P. Kearney [a,*], Lauren M. Porensky [a], David J. Augustine [a], Rowan Gaffney [a,c], Justin D. Derner [b]

[a] USDA-Agricultural Research Service (ARS) Rangeland Resources and Systems Research Unit, Fort Collins, CO 80526, USA
[b] USDA-ARS Rangeland Resources and Systems Research Unit, Cheyenne, WY 82009, USA
[c] UNAVCO, Inc., Boulder, CO 80301, USA

ARTICLE INFO

Keywords:
Harmonized Landsat Sentinel
Image time series
Herbaceous biomass
Vegetation index
Adaptive rangeland management
Grasslands

ABSTRACT

Adaptive management requires rangeland managers to respond to changing forage conditions (e.g., standing herbaceous biomass) within the grazing season at the scale of individual pastures. While within-season biomass can be measured or estimated in the field, it is often impractical to make field measurements in extensive rangeland systems with adequate frequency and spatial representation for responsive decision-making by rangeland managers. We sought to develop a single model to accurately predict daily herbaceous biomass across seasonally and annually varying conditions from the Harmonized Landsat-Sentinel satellite time series. We also sought to assess how information about plant community composition derived from a high-spatial resolution map would improve model performance. We used herbaceous biomass data from 1764 ground observations collected over 8 years in North American shortgrass steppe for training in a cross-validated model selection approach to evaluate (1) predictive performance of candidate models both spatially and temporally, (2) relative variable importance of individual spectral bands, vegetation indices, and recently developed broadband spectral angle indices, and (3) the degree to which including plant community composition improved model performance. All 11 candidate models identified in the model selection procedure contained a band angle index and an individual spectral band, and 6 contained one of each input feature type, demonstrating the benefit of combining spectral features for predicting herbaceous biomass across varying conditions. The spatial and temporal cross-validation and selection procedures produced the same top model with similar performance (mean absolute error = 151–182 kg ha^{-1}; R^2 = 0.75–0.79), suggesting that a single model performs well over space and time. Including plant community composition in the model reduced mean absolute error by 11–13%. Bootstrapping revealed that –six to seven years of training data were required to achieve consistent model performance across years with varying environmental conditions (e.g., wet, average, dry). The top model could accurately detect (70–87% accuracy) the week that biomass dropped below management-related thresholds as low as 450 kg ha^{-1} in an independent dataset (n = 950) with modest commission error (10–26%). We discuss how maps showing the probability that herbaceous biomass is below a given threshold can support adaptive management in extensive semiarid rangelands across differing scenarios of risk perception and avoidance. In addition to producing maps to support precision rangeland management strategies, this study demonstrates the importance of combining complementary vegetation indices and acquiring long-term training datasets to achieve reliable predictions of herbaceous standing biomass in highly variable systems.

1. Introduction

Adaptive management of working landscapes has been proposed as a means to achieve ecological and economic resilience and provide multiple ecosystem services in a changing world (Derner and Augustine, 2016; Holling, 1978; Westgate et al., 2013). In its simplest form,

* Corresponding author.
E-mail address: sean.kearney@usda.gov (S.P. Kearney).

https://doi.org/10.1016/j.rse.2022.112907
Received 19 November 2021; Received in revised form 10 January 2022; Accepted 12 January 2022
Available online 1 February 2022
0034-4257/Published by Elsevier Inc.

adaptive management seeks to improve resource management and reduce uncertainty in social-ecological systems through an iterative process of: (i) monitoring management outcomes, (ii) learning and understanding how systems function, (iii) adjusting underlying assumptions and objectives, and (iv) altering management actions accordingly (Holling and Meffe, 1996; Petersen et al., 2014). Rangelands are well-suited to adaptive management, in part because it is challenging to incorporate the decision-making and learning processes inherent to rangeland management into traditional research frameworks (Wilmer et al., 2018). Globally, rangelands cover greater than 25% of land surface and support a wide range of wildlife and biodiversity while also producing half of the world's livestock (Safriel et al., 2005). They are characterized by frequent disturbances such as grazing and fire in conjunction with variable precipitation. Disturbances and weather variability, combined with grazing management decisions, can shift vegetation composition over time (e.g., Porensky et al., 2017) making it challenging to match forage demand by herbivores with forage supply across grazing seasons (Holechek et al., 1995), thus creating challenges for sustaining both ecological integrity and economic viability.

Adaptive management involves rangeland managers responding to changing forage conditions at spatial scales ranging from individual pastures to entire landscapes (e.g., public management units) and at temporal scales ranging from decadal to interannual and within individual grazing seasons (Fernández-Giménez et al., 2019). Standing forage biomass (i.e., the mass of herbaceous vegetation present at a given point in time) is a key indicator for many rangeland management decisions at all scales. For example, annual decisions may use end-of-season forage biomass and grazing utilization to set livestock stocking rates for the next season, or government agencies may decide where to perform fire mitigation or prescribed burning on public lands based on biomass estimates. Within-season decisions also rely on estimates of standing forage biomass, for example: (a) adjusting rotational grazing strategies (e.g., deciding when to move livestock into different pastures); (b) determining whether to change the length of time livestock graze in a pasture (e.g., avoiding over-grazing or optimizing weight gain); (c) improving rangeland health and d) providing suitable wildlife habitat. Many of these decisions require information on when standing biomass thresholds are reached that would limit livestock productivity, wildlife habitat, or long-term rangeland sustainability (Davis et al., 2020; Fernández-Giménez et al., 2019; Grigera et al., 2007; Wilmer et al., 2018). Furthermore, the ability to monitor how rapidly standing forage biomass declines while being grazed by a known number of livestock can enhance stocking rate decisions by rangeland managers, especially by reducing negative effects of drought (Derner and Augustine, 2016; Díaz-Solís et al., 2009).

While standing biomass can be estimated or directly measured in the field, it is impractical for managers to carry out field sampling across extensive rangeland systems, often covering tens of thousands of hectares or more, with adequate temporal frequency and spatial resolution to capture the spatial-temporal heterogeneity that commonly exists across pastures or management units. Remote-sensing based methods to produce daily or weekly estimates of standing biomass at sub-pasture spatial scales would be highly desirable to facilitate within-season adaptive management. It is important to note here the distinction between standing biomass and total biomass production, often stated as net primary productivity (NPP). Remote-sensing based approaches currently provide valuable bi-weekly maps of annual NPP across large regions at 30-m spatial resolution (Jones et al., 2021). These maps tend to rely on process-based models, incorporating satellite reflectance and meteorological data to accurately predict biomass production to date or forecast total seasonal production (Hartman et al., 2020). However, standing biomass is influenced not only by plant production, but also by losses due to processes such as livestock consumption, trampling, senescence, wildlife herbivory, insects, fire, and weather (e.g., hail). Satellite-based estimates of standing biomass have been made at key periods within the grazing season to enable pasture-scale decision making from year to year, for example by estimating grazing utilization from the previous grazing season to inform stocking rates for the upcoming season (Jansen et al., 2021). However, examples of satellite-based standing biomass predictions applicable to *within*-season management decisions remain sparse (though see Jansen et al., 2018 for an example).

Within-season standing biomass estimates at moderately high spatial resolution (e.g., $\leq$ 30 m) have been challenging to produce for several reasons. Historically, imagery was not available at the appropriate spatial-temporal scales to estimate biomass sub-monthly for individual pastures. Furthermore, arid and semi-arid rangelands exhibit very high heterogeneity in forage conditions from year-to-year, and even within a single growing season, in response to variable precipitation, temperature, soils, and grazing intensities (e.g., Augustine, 2010; Irisarri et al., 2016). In addition, a robust field-based training dataset spanning multiple years and phenological periods is required to obtain ground-based training datasets of forage biomass covering a wide range of forage conditions (e.g., complex mixtures of green and brown vegetation). Finally, even with adequate remote sensing imagery and field-based training data, it is unclear whether a single biomass model can accurately predict forage biomass across the spatially and temporally variable conditions observed in extensive arid and semi-arid rangelands. As an example of temporal model inconsistency, Jansen et al. (2018) found that separate models were required for predicting summer (i.e., green/photosynthetically active) and fall (i.e., brown/senesced) forage biomass from optical Landsat imagery for a C_3 bunchgrass system in eastern Oregon, USA. As a spatial example, Gaffney et al. (2018) found model coefficients were different for shorter-structured C_4 perennial grasses compared to taller-structured C_3 perennial grasses when predicting annual net herbaceous productivity from Landsat-MODIS fusion imagery in the shortgrass steppe of Colorado, USA.

In this study, we first sought to develop a single model to accurately predict within-season (i.e., daily) herbaceous biomass across multiple years from satellite imagery for a North American shortgrass rangeland system. A single model derived from free and public imagery was desirable to enable computationally efficient near-real-time biomass estimation for future efforts. To obtain a temporally dense satellite time series at a spatial scale appropriate for individual pastures, we utilized the Harmonized Landsat-Sentinel (HLS) dataset developed by NASA (Claverie et al., 2018), which provides 30 m optical imagery every 2–3 days. To compile robust field-based data for training and validation, we used biomass estimates from more than 2700 observations collected over 8 years as part of long-term research trials at the Central Plains Experimental Range in the shortgrass steppe. This dataset allowed us to evaluate model performance temporally across the entire grazing season covering a wide range of weather conditions, as well as spatially for new 'unseen' pastures.

We also sought to assess how additional information about vegetation composition would improve model performance. As sensor technologies and computational capacities become more advanced and accessible, spatial information about plant community composition is likewise becoming more readily available (Gaffney et al., 2021; Jones et al., 2018). To understand the utility of such information for improving herbaceous biomass estimation in rangelands, we evaluated whether including a newly developed map of vegetation structure (derived from 1-m airborne hyperspectral imagery) as a co-variate improved model performance. To assess not only how well the models fit the data, but whether they could detect key biomass thresholds used in adaptive decision making, we analyzed the accuracy of each model to predict pasture-scale biomass thresholds used to trigger within-season livestock rotations under an adaptive pulse-grazing management regime (Augustine et al., 2020). Finally, we present examples of how model outputs can be translated into threshold probability products to assess historical and near-real-time conditions to evaluate and inform adaptive management in semiarid rangeland ecosystems.

2. Methods

2.1. Study area

2.1.1. Study area and experimental design

Research was conducted at the Central Plains Experimental Range in northeastern Colorado, USA (40°50′N, 104°43′W), which is a Long-Term Agroecosystem Research network site (Spiegal et al., 2018), a National Ecological Observatory Network site (Keller et al., 2008), and a former Long-Term Ecological Research network site from 1982 to 2012 (Lauenroth and Burke, 2008). Topography is flat to gently rolling; soils range from fine sandy loams on upland plains to alkaline salt flats bordering drainages. Two C_4 shortgrasses – blue grama (*Bouteloua gracilis*) and buffalograss (*B. dactyloides*) – are dominant (Lauenroth and Sala, 1992). C_3 perennial grasses (*Pascopyrum smithii, Hesperostipa comata*, and *Elymus elymoides*), C_4 bunchgrasses (*Aristida longiseta, Sporobolus cryptandrus*), plains pricklypear cactus (*Opuntia polyacantha*), subshrubs (*Gutierrezia sarothrae, Eriogonum effusum, Artemisia frigida*), and saltbush (*Atriplex canescens*) are less abundant but widespread and generate taller structure on the landscape (Augustine and Derner, 2015).

Long-term mean annual precipitation is 340 mm, with >80% occurring April–September (Lauenroth and Burke, 2008). Precipitation is highly variable within and among years (Augustine, 2010) and exerts a strong influence over the timing and magnitude of vegetation productivity and indicators of photosynthetic activity such as the Normalized Difference Vegetation Index (NDVI; see Fig. 1). During our study (2013–2020), two years had above-average precipitation and NDVI (2014, 2015), four years had near-average precipitation and NDVI (2016–2019), one year had below-average precipitation and NDVI (2020) and one year had pulses of precipitation resulting in a multi-modal NDVI signal (2013).

2.2. Ground data

2.2.1. Visual obstruction (VO) aboveground biomass regression model

To create a robust training dataset, we used a rapid, ground-based method for estimating aboveground herbaceous biomass because clipping and weighing biomass from plots is an extremely labor-intensive process. We calibrated a method that estimates aboveground herbaceous biomass from vegetation visual obstruction (VO) measurements, following a modification of the method described by Robel et al. (1970). Briefly, VO readings were conducted by an observer viewing a vertical plastic pole marked with alternating 1-cm black and white bands. Observers recorded the lowest interval on the pole that was not completely obscured by vegetation and the highest band that contained any vegetation partially obscuring it (see Supplemental Material for a detailed description).

We then created a multiple regression equation that estimated aboveground standing biomass (kg ha^{-1}) as a function of the VO readings (see Supplemental Material for detailed methods). Mean clipped aboveground herbaceous biomass was modeled as a linear function of the mean low VO reading ($p < 0.001$) and the mean high VO reading ($p < 0.01$; overall regression: $F_{2,55} = 136.9$, $p < 0.001$), where:

Herbaceous biomass (kg ha^{-1}) = 133.6 * MeanLow (cm) + 23.7 * MeanHigh (cm) + 32.9

with an adjusted $R^2 = 0.83$ (Fig. S1). Inspection of the residuals by

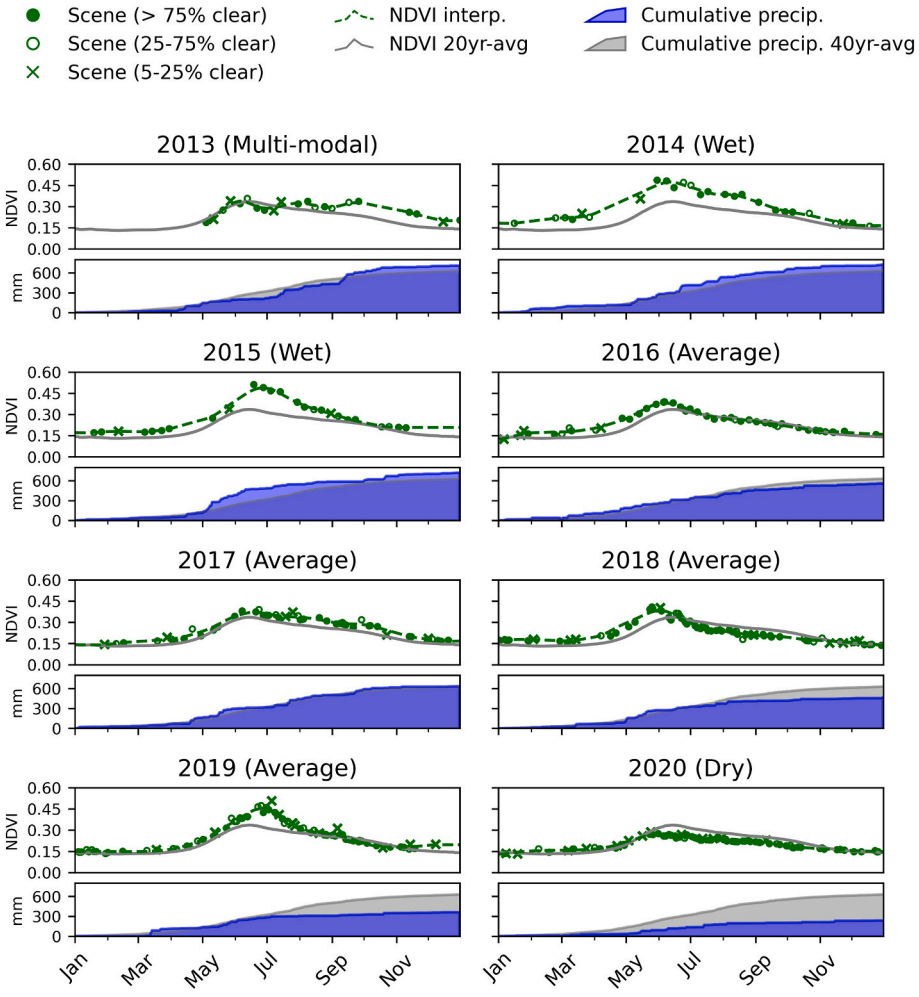

Fig. 1. Time series of HLS-derived NDVI (top panels) and annual cumulative precipitation (mm; bottom panels) from 2013 to 2020 compared to long-term averages for the entire study area. For NDVI, individual HLS scenes are shown as points, with the marker type indicating the percent of the study area that is clear (i.e., free of clouds, shadows, snow and water; scenes with <5% clear not shown). The dashed green line shows the gap-filled and smoothed NDVI curve derived from individual scenes. The solid grey line shows the 20-year mean NDVI derived from Landsat-MODIS fusion (Gao et al., 2015). For precipitation (bottom panels), the blue region show cumulative precipitation for the calendar year and the grey region shows the 40-year mean. (For interpretation of the references to colour in this figure legend, the reader is referred to the web version of this article.)

predicted plot indicated symmetric positive and negative residuals, though with a slight trend for larger residuals when biomass was above 1500 kg ha^{-1}, which occurred rarely in wet years (Fig. S1).

2.2.2. Seasonal VO data for training satellite-based biomass models

We estimated aboveground herbaceous biomass using the VO method at 132 plots distributed across 29 different pastures in mid-June and early October each year during 2013–2020 (not every plot was sampled in every year; sampled $n = 1764$ plots) as part of a collaborative adaptive grazing management experiment (Augustine et al., 2020). Each plot contained a systematic grid of four, 25-m transects oriented north-south and spaced 106 m apart. We measured VO at eight points spaced at 3-m intervals along each transect from two opposite directions perpendicular to the transect (i.e., 16 VO readings per transect; 64 readings per plot).

During the June reading, plant cover was measured along each 25-m VO transect using the line-point intercept method (Herrick et al., 2005), with a laser passed vertically through the vegetation at 50 points distributed at 50-cm intervals. Species of any current-year vegetation contacted by the laser were recorded, as was "standing dead" vegetation produced in the prior year growing season. When no standing vegetation was contacted, we recorded whether the laser contacted bare soil or litter at the ground surface. We calculated plot-scale percent cover of three vegetation types based on the frequency of point observations for each type: percent standing dead, percent litter, and percent bare ground. These cover estimates were used to investigate potential bias in final remote-sensing biomass models (see Section 2.6.1.).

2.2.3. Weekly VO data for validating biomass threshold detection

We estimated biomass from VO measured each week from mid-May to early October in a subset of 79 plots across 11 pastures from 2014 to 2020 (sampled $n = 950$). Each week, VO measurements occurred on four plots within a pasture being grazed by a herd of cattle that was rotated among pastures in response to forage conditions (see Augustine et al., 2020). The weekly measurements occurred along two 50-m transects located between the four permanent transects described previously, and technicians recorded 25 VO readings per transect. Whenever the cattle moved to a new pasture, weekly VO measurements also shifted. Thus, weekly VO measurements encompassed a wide range of vegetation biomass (high when cattle entered the pasture; declining until biomass reached a threshold that was insufficient to support the herd).

2.3. HLS satellite data

The HLS v1.4 dataset contains time series of surface reflectance imagery from the Landsat 8 Operational Land Imager (HLSL30) and Sentinel-2A/B MultiSpectral Instrument (HLSS30) (Claverie et al., 2018). We downloaded all available HLS v1.4 data from April 19, 2013 through December 31, 2020 for the tile covering the study area (13TEF). Sentinel 2A data was only available for the study area beginning October 20, 2015 and Sentinel 2B beginning July 1, 2017. We used smoothing and gap-filling (Section 2.3.3.) in part to account for the fact that temporal coverage of individual scenes was denser in the second half of the study period (Fig. 1).

2.3.1. HLS cloud and shadow masking

Visual assessment showed substantial omission errors of clouds and shadows (most notably shadows) in the native mask included with the HLS product, which was consistent with other studies (e.g., Bolton et al., 2020). Since commission errors were minimal, we retained the native HLS mask and applied two additional masking steps to detect and remove omitted clouds and shadows: (1) the Automatic Time-Series Analysis (ATSA) method developed by Zhu and Helmer (2018), and (2) a temporal filtering and de-spiking method (Bolton et al., 2020). A detailed description of these additional masking steps is provided in the Supplemental Material.

2.3.2. Deriving HLS input features

We identified a suite of HLS-derived candidate model input features designed to capture a wide range of vegetation conditions, including indices and individual bands (Table 1). We chose five vegetation indices, each developed for specific vegetation types: (1) the Normalized Difference Vegetation Index (NDVI) to capture photosynthetically active 'green' vegetation; (2) the Dead Fuel Index (DFI) to capture standing senesced vegetation; (3) the Normalized Difference Tillage Index to capture vegetation residue or litter; and two indices shown to relate to standing vegetation without strong sensitivity to its photosynthetic state, (4) the Soil-Adjusted Total Vegetation Index (SATVI) and (5) the Normalized Difference Infrared Index (NDII7), also called the Normalized Burn Ratio (NBR; see Ji et al., 2011 for terminology).

The DFI, NDTI, SATVI and NDII7 all utilize SWIR bands, which makes them less sensitive to the photosynthetic state of vegetation (i.e., they capture senesced vegetation and residue), but may increase sensitivity to water content of surface soils, vegetation and litter (Quemada

Table 1
Model candidate input features derived from the Harmonized Landsat-Sentinel (HLS) dataset. Formulas for deriving vegetation indices and key sources are provided where applicable. Note that NIR refers to the 0.85–0.88 μm near-infrared band (HLSL30 Band 05 and HLSS30 band 8A).

Feature	Description	Formula	Source
Vegetation indices			
DFI	Dead fuel index	$100^{*}\left(1-\frac{SWIR2}{SWIR1}\right)^{*}\left(\frac{RED}{NIR}\right)$	Cao et al. (2010)
NDVI	Normalized difference vegetation index	$\frac{NIR-RED}{NIR+RED}$	Rouse et al. (1974)
NDTI	Normalized difference tillage index	$\frac{SWIR1-SWIR2}{SWIR\,1+SWIR2}$	Van Deventer et al. (1997)
SATVI	Soil adjusted total vegetation index	$\frac{SWIR1-RED}{SWIR1+RED+0.5}^{*}(1+0.5)-\left(\frac{SWIR2}{2}\right)$	Marsett et al. (2006)
NDII7	Normalized Difference Infrared Index 7 or Normalized Burn Ratio (NBR)	$\frac{NIR-SWIR2}{NIR+SWIR2}$	Hardisky et al. (1983); Ji et al. (2011)
Broadband spectral angle indices (BAIs)			
BAI_126	BAI (BLUE, GREEN, SWIR2)		Yue et al. (2020)
BAI_136	BAI (BLUE, RED, SWIR2)		
BAI_236	BAI (GREEN, RED, SWIR2)		
BAI_246	BAI (GREEN, NIR, SWIR2)		
Individual bands			
NIR	Near-infrared (0.85–0.88 μm)		
SWIR1	Shortwave infrared 1 (1.57–1.65 μm)		
SWIR2	Shortwave infrared 2 (2.11–2.29 μm)		

and Daughtry, 2016; Yue et al., 2020). We therefore also included newly developed broadband spectral angle indices (BAIs) developed by Yue et al. (2020) as potential input variables. The BAIs are less sensitive to surface moisture than traditional vegetation indices when estimating fractional cover of vegetation, crop residue and bare soil in monocot crops. In brief, each BAI uses three of the six HLS bands and is calculated as the angle at the intersection of the line connecting the reflectance of the first and second bands and the line connecting the reflectance of the second and third bands, with the first two bands coming from the visible or NIR range and the third band from the SWIR range (see Supplemental Material and Yue et al., 2020).

Since our ground-based biomass estimates are derived, in part, from vegetation height, we chose to also include three individual bands as candidate input features: NIR, SWIR1 and SWIR2. Bands in the NIR range are inversely correlated with herbaceous vegetation height in grasslands (Marsett et al., 2006). Previous work in our study area (unpublished) indicated the SWIR1 and SWIR2 bands were correlated with biomass and total vegetation cover.

2.3.3. Generating daily time series of HLS input features

We interpolated and smoothed each candidate input feature derived from the HLS time series to generate an image coincident with each ground observation. While interpolation and smoothing are common practice when working with temporally dense satellite time series (e.g., Bolton et al., 2020; Gaffney et al., 2018), there is not a universally standard approach. We chose to apply a two-step Savitzy-Golay smoothing algorithm to individual pixels and separately for each year. In the first step, we used the masked dataset and allowed for non-uniform temporal spacing with a window size of seven datapoints and a third-order polynomial (see Supplemental Material for a Python implementation of the non-uniform smoothing algorithm). In the second step, we applied linear interpolation between all datapoints output from the first step, and then applied the smoothing algorithm again with a uniformly spaced window size of 31 days and a third-order polynomial.

2.4. Species composition map

To represent species composition across the study area, we produced annual maps at 30-m spatial resolution representing the percent cover of mid-height grasses (primarily C_3 species *P. smithii*, *H. comata,* and *E. elymoides*) in each pixel. These maps were derived from plant community classification products available for 2013 and 2017, which classified 1 × 1 m pixels into 10 plant community classes using airborne hyperspectral data (see Gaffney et al., 2021). We converted plant community class maps into a continuous percent midgrass variable (MG-map; see Supplemental Material for description of MG-map derivation) since the ratio of midgrass to shortgrass species is one of the main differences between communities with different biomass-precipitation response patterns in the study area (Irisarri et al., 2016), and percent midgrass would be relatively easy for managers to measure or estimate. The maps were only available for two years; therefore, we used the 2013 map for 2013–2015 and the 2017 map for 2016–2020.

2.5. Modelling

2.5.1. Regression model development

We used a model selection approach to develop linear regression models predicting herbaceous biomass from the HLS features alone (HLS-only) and in combination with the midgrass map (HLS + MG-map). Prior to modelling, we log-transformed biomass (the dependent variable), which had a positively skewed distribution. For each plot, we extracted the mean value for each HLS feature on the date the plot was sampled. To extract plot means, we created a minimum convex hull polygon around the four transects sampled in each plot and buffered the polygon by 15 m, resulting in a mean plot size of 22.2 ha (s.d. = 0.11 ha), or approximately 25 HLS pixels. We also extracted the mean percent midgrass value for each plot from the species composition map.

First, we produced all possible combinations of regression models that contained up to six HLS input features and did not contain any HLS input features with a Pearson correlation >0.8. We included two-way interactions between HLS input variables in all models and used these as the set of available models using only the HLS features (HLS-only). For the models combining HLS features and the species composition map (HLS + MG-map), we followed the same steps and then included the percent midgrass as an additional variable in each model, allowing for two-way interactions between percent midgrass and each of the HLS features present in the model. The complete set of available models included 569 models for each of the two types (HLS-only and HLS + MG-map).

2.5.2. Temporal and spatial cross-validation

We evaluated model performance both temporally and spatially using two separate cross-validation procedures. For temporal evaluation, we used a 'leave one group out' cross-validation procedure which iteratively held out all data from a single year (testing data), built each regression model from the other seven years (training data), and evaluated it on the holdout year. For spatial evaluation, we used a grouped k-fold iterator with non-overlapping groups set as individual pastures, which ensured that plots from the same pasture where never included in both the training and test datasets. We set k = 8 to match the number of iterations (i.e., years) used for temporal cross-validation.

For each model, we produced metrics of model error, bias, and fit. We calculated model error as the mean absolute error (MAE; absolute value of predicted minus observed values) of the testing data, and present MAE for the log-transformed biomass (Log kg ha^{-1}), the back-transformed biomass (kg ha^{-1}) and as a percent of the mean back-transformed biomass (%). We calculated bias as the mean percent error (MPE; predicted minus observed values, divided by the observed value) of the back-transformed biomass, where positive values indicate over-prediction and negative values indicate under-prediction. We evaluated model fit using R^2 and Akaike Information Criterion weights (AIC_w) of the trained model. AIC_w represents the relative likelihood of a model being the 'true' model compared to the model with the lowest AIC score, and values can range from 0.0–1.0 (Burnham and Anderson, 2002).

For all metrics, we calculated the mean and standard deviation for each model across all cross-validation iterations. For AIC_w, we also calculated the maximum AIC_w for each model across all iterations to be used in model selection.

2.5.3. Model selection

We considered any model with an $AIC_w > 0.5$ in at least one cross-validated iteration as a candidate model that performed well across our dataset. We ranked these candidate models based on the MAE of the back-transformed biomass (kg ha^{-1}) and selected the candidate model with the lowest MAE for further analysis (see Section 2.6). All candidate models based on temporal and spatial cross-validation are presented in Tables 2 and 3, respectively.

2.5.4. Variable importance

To understand the relative variable importance (RVI) of each of the HLS features and percent midgrass for predicting herbaceous biomass, we calculated a model-weighted partitioned R^2 for each input variable across all models (Giam and Olden, 2016). First, for a given variable x, we calculated the partitioned R^2 (RVI_x) as the average increase in R^2 for a given model k compared to the R^2 of an otherwise identical model omitting that variable (k_{-x}). This RVI was then weighted by the AIC_w of the model k that included the variable and summed across all models containing the variable x, calculated as:

Table 2
Candidate model subsets using temporal cross-validation. Candidate models had a maximum AICw ≥0.5. Top model is highlighted in bold and was chosen based on having the lowest mean absolute error (MAE) on the log scale (i.e., the model dependent variable).

Formula (simplified)	Mean Absolute Error (MAE)						Bias		Model fit				
	Log kg ha^{-1}		*kg ha^{-1}*		*Relative (%)*		*Mean % Error*		*AICw*		*Max AICw*	*Adj-R^2*	
HLS features only													
Y ~ NDII7 + NIR + BAI_236	**0.2107**	**(0.0355)**	**182.28**	**(43.71)**	**20.7%**	**(3.2%)**	**5.1%**	**(12.9%)**	**0.23**	**(0.35)**	**0.96**	**0.75**	**(0.03)**
Y ~ NIR + SWIR2 + BAI_136	0.2114	(0.0366)	183.38	(43.69)	20.9%	(3.3%)	4.9%	(12.6%)	0.50	(0.43)	0.93	0.75	(0.03)
Y ~ DFI + SWIR2 + BAI_126	0.2154	(0.0318)	183.33	(42.19)	20.8%	(2.8%)	5.8%	(13.0%)	0.14	(0.35)	1.00	0.74	(0.03)
HLS features + midgrass (MG-map)													
Y ~ NDII7 + NIR + BAI_236 + MG-map	**0.1904**	**(0.0383)**	**161.78**	**(41.72)**	**18.4%**	**(3.4%)**	**4.7%**	**(11.9%)**	**0.31**	**(0.42)**	**0.97**	**0.79**	**(0.02)**
Y ~ SWIR2 + BAI_136 + BAI_246 + MG-map	0.1926	(0.0328)	165.21	(41.47)	18.8%	(2.8%)	4.3%	(11.6%)	0.27	(0.42)	0.97	0.79	(0.02)
Y ~ DFI + SWIR2 + BAI_126 + MG-map	0.1964	(0.0347)	166.17	(43.53)	18.8%	(3.0%)	5.1%	(11.6%)	0.12	(0.35)	0.98	0.79	(0.03)
Y ~ SWIR2 + BAI_136 + BAI_246 + MG-map	0.1926	(0.0328)	165.21	(41.47)	18.8%	(2.8%)	4.3%	(11.6%)	0.27	(0.42)	0.97	0.79	(0.02)

Table 3
Candidate model subsets using spatial cross-validation. Candidate models had a maximum AICw ≥0.5. Top model is highlighted in bold and was chosen based on having the lowest mean absolute error (MAE) on the log scale (i.e., the model dependent variable).

Formula (simplified)	Mean Absolute Error (MAE)						Bias		Model fit				
	Log kg ha^{-1}		*kg ha^{-1}*		*Relative (%)*		*Mean % Error*		*AICw*		*Max AICw*	*Adj-R^2*	
HLS features only													
Y ~ NDII7 + NIR + BAI_236	**0.2014**	**(0.0163)**	**173.87**	**(25.50)**	**20.6%**	**(5.8%)**	**3.4%**	**(8.9%)**	**0.54**	**(0.38)**	**0.99**	**0.75**	**(0.01)**
Y ~ NIR + SWIR2 + BAI_136	0.2018	(0.0161)	174.92	(26.64)	20.7%	(5.8%)	3.5%	(8.7%)	0.43	(0.40)	0.99	0.75	(0.01)
HLS features + midgrass (MG-map)													
Y ~ NDII7 + NIR + BAI_236 + MG-map	**0.1789**	**(0.0181)**	**151.15**	**(21.37)**	**18.2%**	**(6.3%)**	**3.0%**	**(6.0%)**	**0.66**	**(0.35)**	**0.99**	**0.79**	**(0.01)**
Y ~ NIR + SWIR2 + BAI_136 + MG-map	0.1800	(0.0170)	153.21	(21.31)	18.4%	(6.5%)	3.0%	(6.1%)	0.23	(0.28)	0.79	0.79	(0.01)

$$RVI_{w_x} = \sum_{k=1}^{K} RVI_{x_k}\left(AIC_{w_k}\right)$$

$$RVI_{X_{jk}} = {R^2}_k - {R^2}_{k_{-x}} \quad (3)$$

where RVIw_x is the weighted relative variable importance of variable x.

2.6. Model analyses and application for adaptive management

For a model to effectively support adaptive within-season decision making the model should (1) perform consistently well across varying rangeland conditions, such as seasonal conditions (e.g., photosynthetic state), annual climate (e.g., wet vs. dry) and vegetation cover (e.g., bare ground, plant community composition); and (2) accurately detect herbaceous biomass thresholds used to trigger decisions to move cattle within an adaptive, multi-paddock rotational grazing management regime (Augustine et al., 2020; Wilmer et al., 2018). The following sections describe additional analyses conducted on the top HLS-only and HLS + MG-map models.

2.6.1. Model consistency across varying conditions

To look for bias in model performance across different years and seasons, we produced violin plots of the residuals of predicted biomass by sampling year and season (i.e., June and October). We also used a bootstrapping approach to understand how model performance for new 'unseen' years changed depending on conditions and the number years in the training dataset. The bootstrapping approach iteratively retrained the final top models with all possible combinations of sampling years using one to seven years of training data. For each iteration, we calculated relative MAE (%) on each of the years not included in the training data. We created boxplots of the relative MAE for each number of years of training data and the mean relative MAE for each individual year and compared how the change in relative MAE with increasing numbers of training years differed when evaluated for dry, average, wet and multi-modal years (see Fig. 1).

To evaluate bias in model performance across vegetation cover conditions, we produced scatter plots of the residuals of biomass predicted from top models by percent midgrass derived from the VO ground data based on the plot-scale frequency of individual point observations where the species responsible for the 'low' reading was a midgrass species. We also looked at how residuals compared to the three cover types – standing dead vegetation, litter, and bare ground – derived from the line-point intercept observations conducted during the June sampling period each year.

2.6.2. Detecting biomass thresholds in pulse-grazed pastures

We compared model-predicted biomass to the weekly VO-derived biomass collected in pulse-grazed pastures from 2014 to 2020. This weekly VO dataset was not used in model training or selection and provides an independent temporal validation. For each week in the VO dataset, we produced a map of model-predicted biomass and extracted the mean value for each weekly VO plot. Next, we identified whether model-predicted and VO-derived biomass were below each of five herbaceous biomass thresholds: 330, 450, 560, 700 and 1120 kg ha^{-1}. We then calculated accuracy, omission, and commission errors by comparing whether the model-predicted biomass was below each threshold in the same week that VO-derived biomass was below each threshold.

Since discrete thresholding does not capture the degree to which a value is close to the threshold, we also created probability maps repre-

senting the probability that the biomass of a pixel is less than or equal to a given threshold. We used a cumulative distribution function and the standard error of the model-predicted biomass.

$$P\ (B_x \leq t) = CDF(z)$$

$$z = \frac{t - B_x}{S_x} \tag{4}$$

Where B_x is the model-predicted biomass for pixel x, S_x is the standard error of B_x and t is the biomass threshold (thus, z is the standardized z-score of the difference between t and B_x).

3. Results

3.1. Modelling

3.1.1. Model selection for remote sensing of herbaceous biomass

Increasing the number of HLS input features beyond three resulted in increasing model error, despite continued improvement in model fit (Fig. S3 and S4). We therefore did not consider models with more than three HLS input features as valid candidate models for final model selection (Table 2 and Table 3) and recalculated AIC_w using only models with ≤3 HLS input features (retaining the two-way interactions). This new model set included 207 possible models.

Using temporal cross-validation, the top HLS-only model had a back-transformed MAE of 182.3 kg ha^{-1} (20.7% relative MAE), while the top HLS + MG-map model had an MAE of 161.8 kg ha^{-1} (18.4% relative MAE). In both cases, the top models (i.e., lowest mean MAE across validation runs), included the same three HLS input features: NIR, NDII7 and BAI_236. Notably, these three features represent all three input feature types: an individual spectral band (NIR), a vegetation index (NDII7) and a broadband spectral angle index (BAI_236). Both models had a slight bias toward overprediction (5.1% and 4.7% mean error, respectively) and good model fit (mean R^2 of 0.75 and 0.79, respectively).

The same top models were selected using spatial cross-validation, and MAE and bias were slightly lower than the temporally cross-validated values (Table 3). Compared to the HLS-only model, the HLS + MG-map model reduced spatially cross-validated MAE by 22.7 kg ha^{-1} (13.1%) and temporally cross-validated MAE by 20.5 kg ha^{-1} (11.2%).

The final two models – selected for having the lowest MAE of all

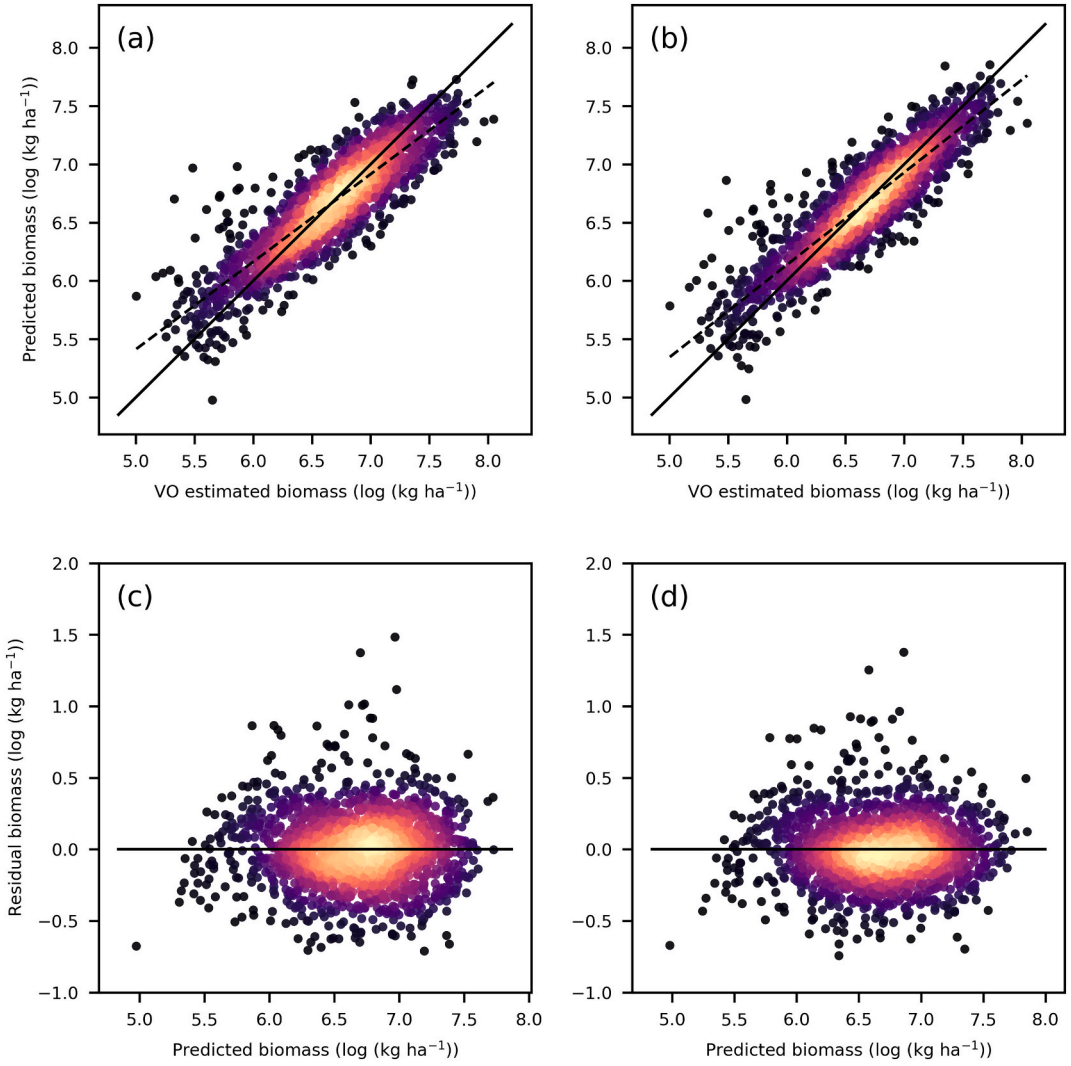

Fig. 2. Top row shows scatterplots of model-predicted versus ground-based biomass estimated from visual obstruction (VO) for (a) the top model using HLS features only ($y = 1.6546 + 0.7515\times$; R^2-adj = 0.75; $p < 0.001$) and (b) the top model using HLS features + MG-map ($y = 1.3770 + 0.7932\times$; R^2-adj = 0.79; $p < 0.001$). Solid line is the 1:1 fit, and dashed line is the linear regression fit. Bottom row shows scatterplots of residual biomass versus model-predicted biomass for (c) the top model using HLS features only and (d) the top model using HLS features + MG-map. Note that all biomass values are shown on the natural log scale. Brighter colors denote a higher density of overlapping points.

candidate models (HLS-only: $Y \sim NDII7 + NIR + BAI\_236$; HLS + MG-map: $Y \sim NDII7 + NIR + BAI\_236 + MG\text{-}map$) – showed high correlation between observed and predicted values and homoskedasticity of residuals when fit with the full dataset (Fig. 2). Both models showed a slight bias toward under-predicting high biomass after back-transformation (Fig. S5), though bias was less pronounced in the HLS + MG-map model.

When evaluated on the independent weekly VO-based biomass estimates in pulse grazed pastures, the top HLS-only model had an MAE of 199.4 kg ha^{-1} (23.3%) and the top HLS + MG-map had an MAE of 186.0 kg ha^{-1} (21.7%). Coefficients for both models can be found in Tables S1 and S2 of the Supplemental Material.

3.1.2. Variable importance

Weighted relative variable importance (RVI_w) was highest for SWIR2, NIR and NDII7, regardless of whether MG-map was included in the model and whether model weights were calculated from temporal or spatial cross-validation (Fig. 3). The RVI_w for the MG-map variable ranked 4th using both spatial and temporal validation. The other HLS features tended to have low RVI_w regardless of whether MG-map was included or temporal or spatial cross-validation was used. The ranking of variable importance among the BAIs changed depending on whether MG-map was included in the model and whether cross-validation was spatial or temporal, though RVI_w tended to be lowest for BAI_126. In general, most BAIs did tend to have higher RVI_w than the remaining spectral bands and vegetation indices (Fig. 3).

3.1.3. Model consistency across varying conditions

Violin plots of residuals by year and by season (June vs. October) showed no consistent bias in predictions by year or by season (Fig. 4). However, patterns observed for individual year-by-season interactions included over-prediction (positive residuals) being more common in October 2013, June 2015 and, to a lesser extent, June 2016 and 2017. When using the HLS + MG-map model, this tendency was less pronounced for June 2016 and 2017, but remained in October 2013 and June 2015.

Bootstrapping revealed that, when predicting on unseen years, mean relative MAE (across all unseen years) declined rapidly from ~35% to ~23% when the number of training years increased from one to four, and then declined more slowly to a low of about 20% with seven years of training data (Fig. 5). However, this pattern was not consistent across annual productivity gradients. Relative MAE tended to be lowest when predicting biomass for years with 'average' precipitation conditions, with relative MAE falling to ~20% with just two years of training data in three out of the four 'average' years. By contrast, when predicting biomass in the two 'wet' years (i.e., high productivity), mean relative

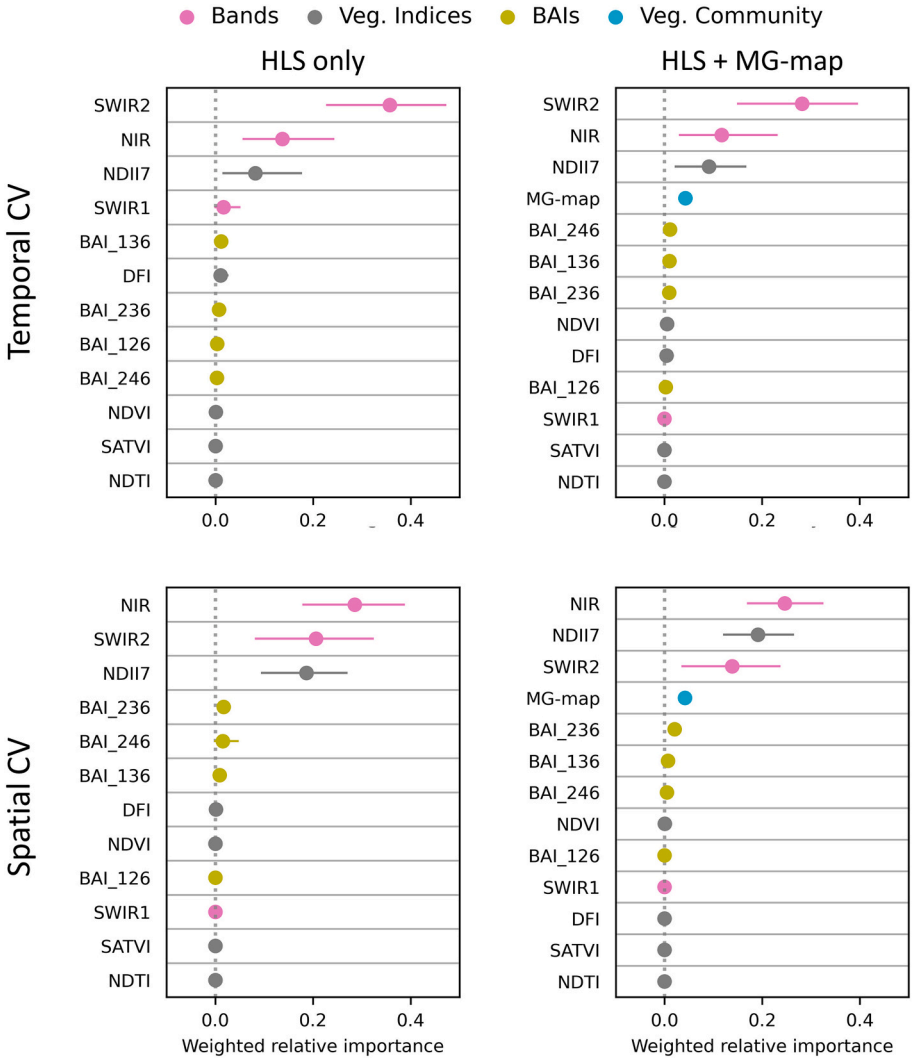

Fig. 3. Weighted relative variable importance (RVI_w) for all model subsets. Top row shows RVI_w using temporal cross-validation and bottom row is based on spatial cross-validation. Left column is RVI_w with HLS features only (individual bands, vegetation indices and broadband spectral angle indices [BAIs]; see Table 1) and right column is RVI_w with HLS features and percent cover of midgrasses mapped from hyperspectral imagery (MG-map) as a representation of the vegetation community.

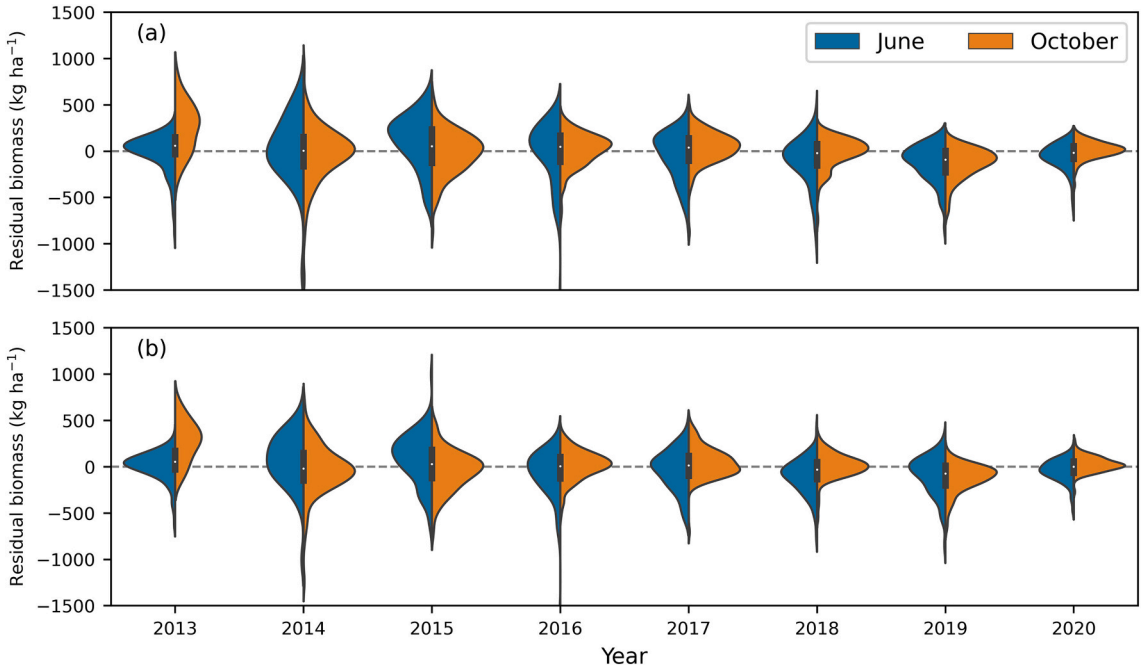

Fig. 4. Violin plots by year and season (June and October) of model-predicted residual biomass (predicted minus observed values) from (a) HLS features only and (b) HLS features + MG-map.

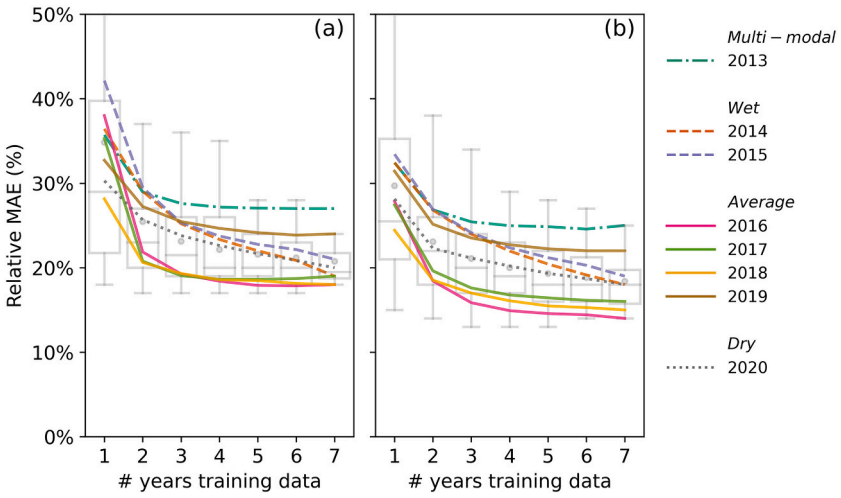

Fig. 5. Bootstrapped performance of final models re-calculated with increasing numbers of years of training data for (a) model derived from HLS features only and (b) model derived from HLS features and percent cover of midgrasses mapped from hyperspectral imagery (MG-map). Boxplots show the distribution of relative mean absolute error (MAE; back-transformed scale) when predicting for all 'unseen' holdout years. Horizontal lines in the boxes show the overall median and points within the boxes show the overall mean. Individual colored lines represent the mean MAE when the year indicated is the holdout 'unseen' year. Line colors represent individual years and line dashing indicates whether the year was average, wet, dry, or multi-modal compared to the long-term average.

MAE tended to be higher (35–45%) with less than five years of training data and continued to decline more linearly compared to 'average' years, requiring seven years of training data to reach the overall mean relative MAE across all years. For the one 'dry' year in the dataset (2020), relative MAE declined in a near-linear fashion from ~30% to ~20% as the number of training years increased from one to seven. For the 'multi-modal' year (2013), relative MAE leveled off at 28–30% once three years of training data were included, with little improvement from additional training years. All patterns were similar regardless of whether MG-map was included in the model, though adding MG-map tended to reduce relative MAE by about 2–4% for most bootstrap iterations.

Scatterplots of model residuals by VO-derived percent midgrass (MG-plot) revealed a moderate negative linear relationship (R^2-adj = 0.27; $p < 0.001$) for the top HLS-only model (Fig. 6a). The model tended to over-predict biomass when precent midgrass was less than ~20% and under-predict biomass when percent midgrass was greater than ~50%. This relationship was less pronounced for the top HLS + MG-map model, though still significant (Fig. 6b; R^2-adj = 0.07; $p < 0.001$). Correlations between residuals and percent cover of standing dead vegetation and bare ground were significant but weak for both models (R^2-adj ≤ 0.06), while correlations with percent cover of litter were not significant for either model (Fig. S6).

3.2. Detecting biomass thresholds in pulse-grazed pastures

Weekly biomass predicted from the HLS-only model followed similar trends to the ground-based weekly biomass measurements (Fig. 7). In most pastures and years, the mean model-predicted biomass was within the range of all plot-scale ground estimates for a given pasture.

For thresholds ≥450 kg ha^{-1}, both models predicted weekly biomass below thresholds with relatively high accuracy (70–87%; Table 4). For the lowest threshold (330 kg ha^{-1}), accuracy of predicting the week when biomass fell below the threshold was poor for both models (17%), however it is important to note there were only six such observations

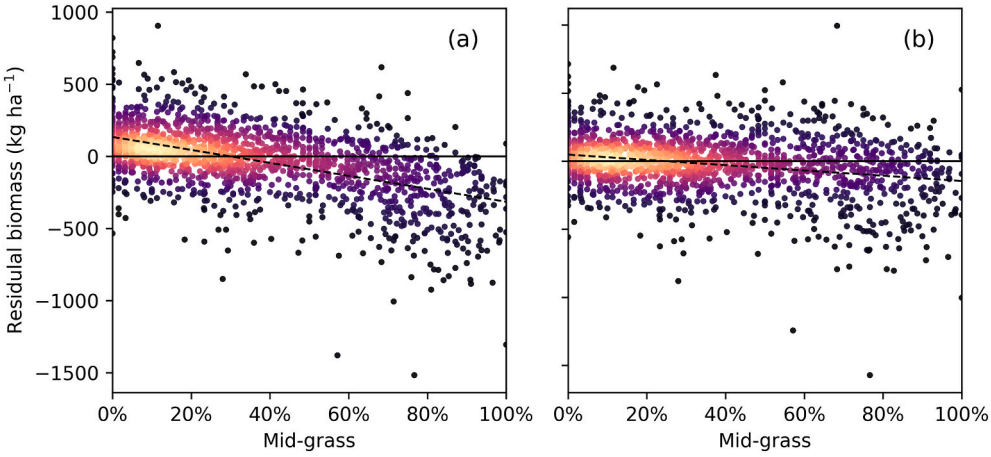

Fig. 6. Scatterplots of model-predicted residual biomass versus VO-derived percent mid-grass (i.e., plot-level frequency of 'low' VO readings for mid-grass species) measured in June and October for (a) the top HLS-only model (y = 134.21–449.22×; R^2-adj = 0.27; $p < 0.001$) and (b) the top HLS + MG-map model (y = 78.16–193.80×; R^2-adj = 0.07; $p < 0.001$). Brighter colors denote a higher density of overlapping points. The dotted line represents the linear regression fit.

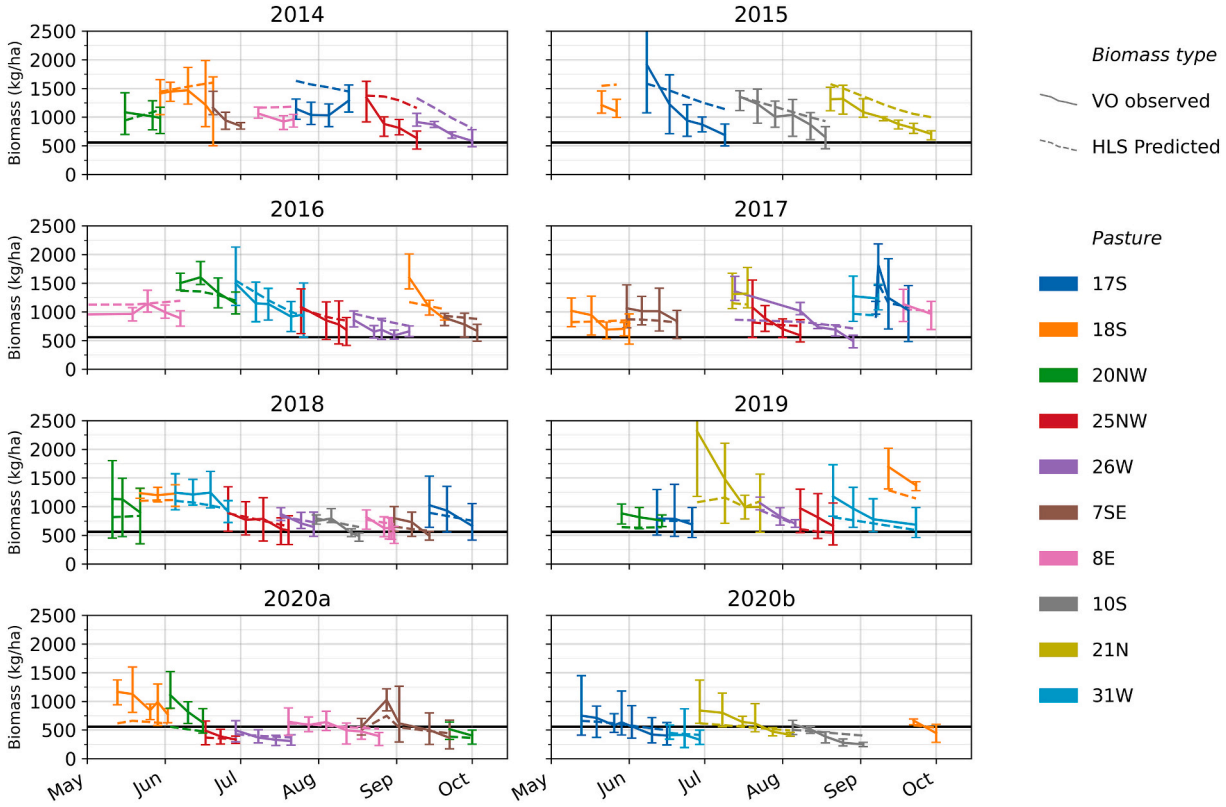

Fig. 7. Weekly biomass observations from pulse-grazed pastures. Solid lines are ground-based biomass estimated with visual obstruction (VO) poles and error bars are the minimum and maximum across plots within a given pasture. Dotted lines are the model-predicted biomass using HLS features. Note that data was available for two separate herds in 2020 and each herd is shown in a separate panel to improve readability.

across the entire dataset. Compared to the HLS-only model, the HLS + MG-map model did not consistently improve the accuracy of predicting whether a pasture was below a given biomass threshold on a given week (Table 4; Fig. 8).

Calculating the probability of a pasture's biomass being below a given threshold shows the trade-offs between commission and omission error when seeking to identify a discrete threshold (Fig. 8). At the example threshold of 560 kg ha^{-1}, as the probability cut-off became more 'stringent' (i.e., probability >0.5), commission error decreased to zero with only a modest increase in omission error. Conversely, as the probability cut-off became less stringent (i.e., lower probability) omission error decreased, but commission error increased rapidly, suggesting that it is impractical to expect to reduce omission error to zero at this threshold. Mapping the probability of biomass being below a threshold showed distinct relationships to rangeland management-associated features at certain times of year (Fig. 9).

Table 4
Accuracy and error for each model when predicting whether weekly pasture-scale biomass was below a given threshold. Note that the number of pastures (n) below a given threshold varies depending on the threshold value assessed.

Threshold (kg ha $^{-1}$)	n < threshold	Threshold accuracy	Omission error	Commission error	Overall accuracy
HLS features only					
330	6	17%	83%	67%	95%
450	23	74%	26%	15%	94%
560	38	87%	13%	20%	93%
700	75	72%	28%	26%	80%
1120	169	85%	14%	10%	80%
HLS features + midgrass (MG-map)					
330	6	17%	83%	67%	95%
450	23	70%	30%	16%	94%
560	38	82%	18%	18%	92%
700	75	77%	23%	25%	82%
1120	169	86%	13%	10%	81%

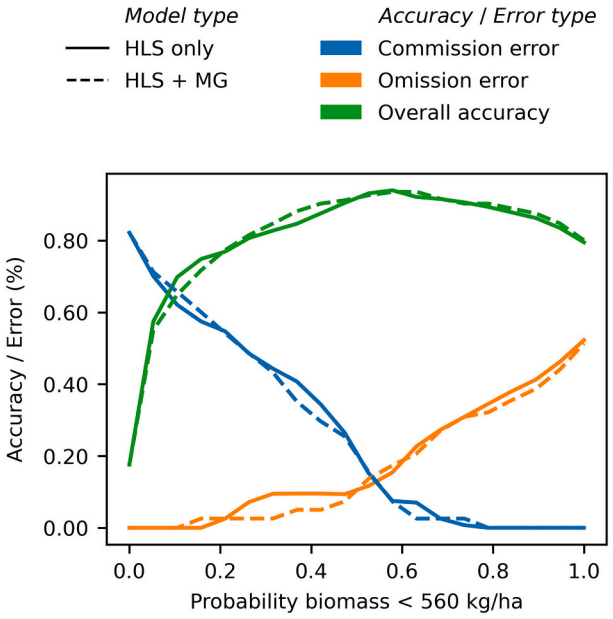

Fig. 8. Demonstration of how overall accuracy, omission error and commission error of detecting the week that biomass in a pasture dropped below 560 kg ha^{-1} changes when using different probability thresholds for detection. The probability is calculated from the model-predicted biomass and standard error of prediction. Pastures were identified as being below 560 kg ha^{-1} if their predicted probability of biomass <560 kg ha^{-1} was less than the probability shown on the x-axis.

4. Discussion

4.1. Herbaceous biomass prediction from satellite in the shortgrass steppe

Our HLS-based modelling approach produced effective near-real-time and historical estimates of standing herbaceous biomass throughout the grazing season for semiarid shortgrass rangelands in North America. Top models had low error (relative MAE of 18–21%) and good model fit (R^2 0.75–0.79) when predicting across a wide range of conditions, likely due in part to the large training dataset in our study, which encompassed high amounts of naturally occurring spatial-temporal variation. The rapid VO method and a long-term research approach were critical for developing a training and validation dataset with robust spatial and temporal coverage.

It is difficult to compare our results to other studies. Remote sensing applications in rangeland biomes remain underrepresented (Reinermann et al., 2020) and, to our knowledge, most other studies seeking to model standing herbaceous biomass with satellite imagery have had limited temporal replication for validation, therefore limiting their ability to validate on 'unseen' years. A review by Reinermann et al. (2020) found that remote-sensing models of production in grazing lands, which include rangelands, had R^2 values ranging from 0.4 to 0.97 but noted that the highest accuracies were for datasets with limited spatial-temporal heterogeneity, or where models were developed for certain seasons. Lower performance of multi-season models is likely due to a reliance on NDVI. The relationship between NDVI and herbaceous biomass can change substantially throughout the growing season as vegetation progresses through its phenology (Edirisinghe et al., 2011; Smith et al., 2011; Wehlage et al., 2016). Consistent with our results, Jansen et al. (2018) and others (e.g., Chen et al., 2011; Numata et al., 2008) determined that indices utilizing spectral reflectance in the SWIR region (e.g., NDII7, NDTI) performed better than NDVI when predicting standing herbaceous biomass in situations where substantial senesced vegetation is present.

Indeed, the importance of using SWIR-based vegetation indices and BAIs in combination with individual spectral bands was apparent in our model selection results. The only vegetation indices present in candidate models utilized the SWIR bands. Furthermore, all eleven candidate models included an individual band (NIR or SWIR2) combined with at least one of the other two feature types, and six out of eleven candidate models included one of each type, including the top models (NIR + NDII7 + BAI_236) in each cross-validation procedure (Table 2; Table 3). This combination of input features likely integrates the spectral response of vegetation cover and height, both of which are related to herbaceous biomass in grasslands (Liang et al., 2016; Marsett et al., 2006) and are captured in the VO ground readings. For example, while the two indices (NDII7, BAI_236) have been shown to be related to vegetation cover (Daughtry et al., 2006; Yue et al., 2020), some studies have found that individual NIR and SWIR2 bands are better predictors of vegetation height in grasslands compared to vegetation indices (Marsett et al., 2006; Yin et al., 2020), though efforts to estimate height of vegetation in grazing lands from satellite are limited. The relationship between individual NIR/SWIR bands and grassland vegetation height may be at least partly explained by recollision probability, whereby taller structured vegetation (e.g., elongated stems, narrow leaves) may allow a greater chance that photons will penetrate the canopy and interact with vegetation, thus decreasing reflectance in NIR and SWIR regions, which is otherwise relatively high for vegetation (Ollinger, 2011). Indeed, we observed strong negative correlations between VO-derived biomass and NIR and SWIR bands (Fig. S7).

The combination of all three feature types in the final models may be particularly useful for capturing height and cover (i.e., biomass) across broad phenological and moisture conditions. While NDII7 and other SWIR-based indices are sensitive to vegetation cover across a range of phenological conditions, they are also sensitive to surface moisture (Quemada and Daughtry, 2016). The BAIs, which were present in all top models, have been shown to be less sensitive to surface moisture when estimating crop residue cover (Yue et al., 2020) and are likely helping to account for varying moisture conditions throughout the season. To our knowledge, this study is the first to utilize BAIs to model herbaceous biomass.

4.2. Vegetation composition as a co-variate

We found that including information about vegetation composition (MG-map) garnered modest improvements in model fit (R^2 increase of 0.04) and accuracy (error reduction of 11–13%). This improvement is consistent with the few other studies that have included vegetation composition as a co-variate or developed species-specific models to estimate grassland biomass from remotely sensed imagery. Magiera et al. (2017) found that including a species composition map reduced grassland biomass prediction error by about 8% and improved R^2 from 0.42

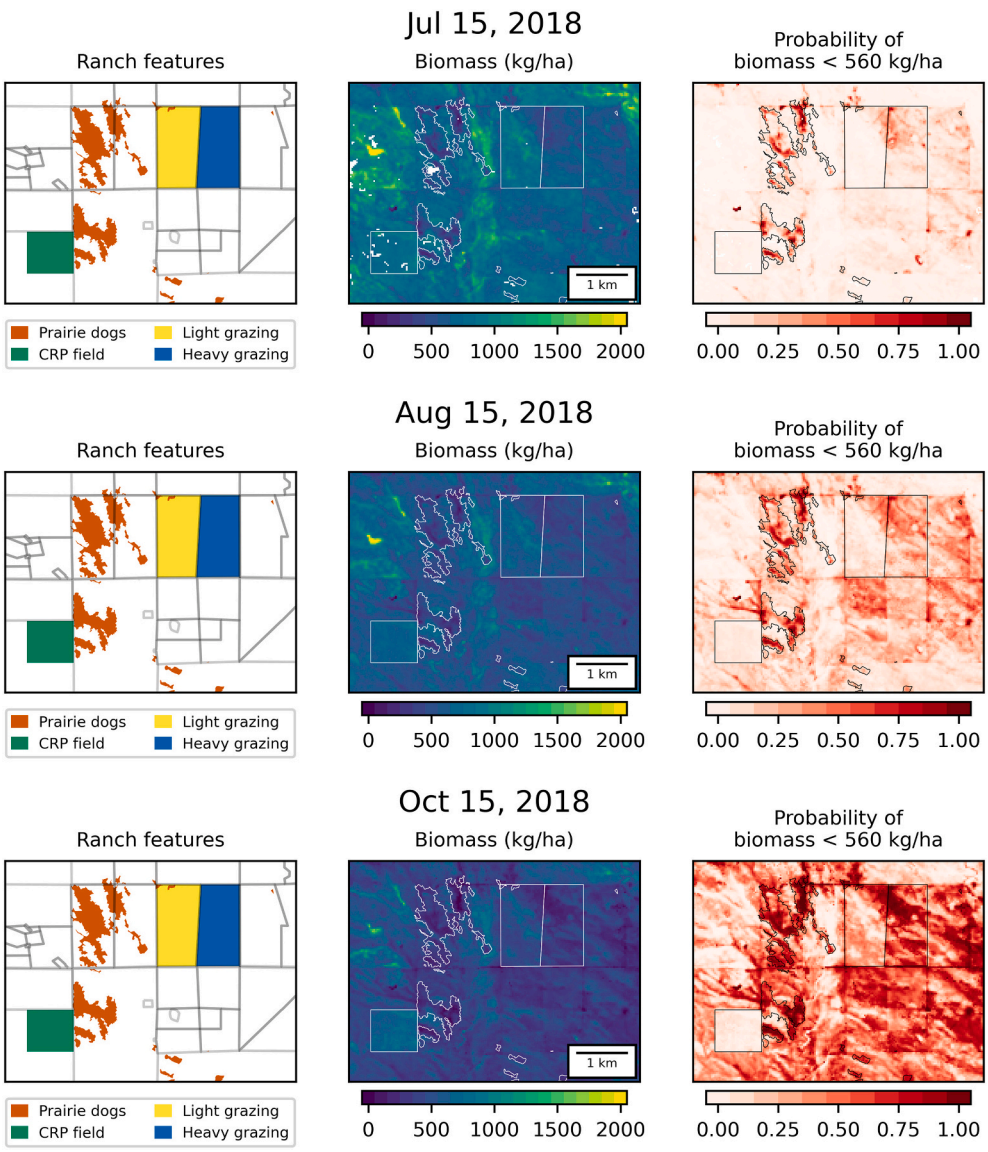

Fig. 9. The left column shows four ranch features identified in 2018 (an 'average' year) within a subset of the study area: prairie dog colonies (orange), pasture lightly grazed at low stocking density (yellow), pasture heavily grazed at high stocking density (blue) and an ungrazed pasture in the Conservation Reserve Program (CRP; green). The center column shows model-predicted biomass (HLS features only) on three separate dates overlayed with the outlines of the four ranch features. The right column shows the probability that biomass is less than 560 kg ha^{-1} on the same three dates, overlayed with outlines of the four ranch features. White pixels in the center and right columns of the top row denote missing data. (For interpretation of the references to colour in this figure legend, the reader is referred to the web version of this article.)

to 0.55 when added to a Random Forest model using RapidEye bands, vegetation indices, and topographic variables. Numata et al. (2008), found that models predicted aboveground biomass from field spectrometer data better for a short homogenous structured grass species than for taller and more complex structured grass (R^2 0.60 vs. 0.38). The improvement was even more pronounced when predicting senesced biomass (R^2 0.70 vs. 0.31).

In our study, the improvements from including MG-map were realized primarily when predicting high biomass values. The HLS-only model tended to under-predict biomass when VO-derived percent midgrass was high (Fig. 6a). This tendency corroborates previous work suggesting that midgrasses in our system are capable of producing more biomass per unit of cover, greenness, and precipitation than shortgrasses (Gaffney et al., 2018; Irisarri et al., 2016). Magiera et al. (2017) also found that including species composition primarily improved model fit at high biomass ranges and for taller structured grasses. Thus, we conclude that it may be more important to include vegetation composition in biomass models for structurally complex grasslands in which compositional heterogeneity is strongly related to variability in herbaceous biomass production potential, and less important for more structurally homogeneous grasslands in which different species produce similar levels of biomass per unit of cover or greenness. This finding is valuable for future mapping efforts given that species composition maps are not readily available across wide spatial and temporal extents. In our study area, the HLS + MG-map model did not substantially improve detection of low biomass thresholds, and as a result may not be necessary for adaptive management decisions related to moving cattle out of a pasture when forage biomass declines below a certain level (see Section 4.3). Other monitoring activities, such as fire fuels estimation or modelling habitat of ground-nesting birds that require tall-structured vegetation, would likely benefit more from incorporating species composition maps to achieve better accuracies in high biomass areas.

4.3. Prediction consistency across varying conditions

Our results highlight the importance of including multiple years of training data that span the range of real-world variation in conditions to achieve reliable model performance (Fig. 5). Our models could not always be reliably extrapolated to years with anomalous conditions when only a few years were included in the training dataset. This finding serves as a caution for applications that use models trained with data from just one or a few years and apply it to other years (e.g., Zhang et al., 2016). This issue is particularly important in arid and semi-arid rangelands and other ecosystems where precipitation patterns and associated

herbaceous biomass production dynamics are highly variable within and between years.

Our study suggests that even with multi-year training datasets, model performance will vary with conditions. Most notably in our study, errors for years with average and consistent precipitation tended to decline more rapidly with additional training data than errors for years with high, low or temporally uneven precipitation (Fig. 5). For years with average and consistent precipitation, error decreased rapidly with additional training data and leveled off at a low rate (MAE < 20%) with 3+ years of training data. The wet (2014, 2015) and dry (2020) study years showed a continued linear decline in error with 3+ years of training data. Finally, for the two study years with the most temporally uneven precipitation distribution (2013, 2019), error leveled off at a relatively high value with 3+ years of training data. One of these years (2013) had highly variable 'pulses' of precipitation and multimodal NDVI growth curves, while the other year (2019) had a wet spring and a very dry late summer (Fig. 1). It is not clear whether the temporally uneven precipitation directly caused reduced model performance for these two years or why that would be the case. In 2013, results are confounded by the fact that the HLS imagery is sparser since Sentinel 2 imagery was not yet available and persistent clouds were present late in the grazing season. However, 2014 and 2015 were also pre-Sentinel 2 and relatively wet and cloudy, again resulting in sparser image coverage (Fig. 1), yet model performance continued to improve with more years of training data. By contrast, 2019 had full 2–3 day repeat image acquisition, yet performance did not improve with 3+ years training data. It is possible that years with temporally uneven precipitation result in more anomalous vegetation conditions, such as unusually high amounts of senesced biomass (e.g., the second half of the 2019 growing season), a senesced or flowering overstory with green understory, or substantial cover of annually variable subdominant vegetation types such as forbs and annual grasses. Such situations may produce spectral conditions not seen in the training dataset, even with seven years of training data.

4.4. Accurate and timely biomass prediction for adaptive decision-making

Recent development of tools such as the Rangeland Analysis Platform (RAP) and the Rangeland Performance Monitoring Service provide valuable maps of vegetation cover types and annual net primary production across the western United States (Jones et al., 2021). However, adaptive decisions on cattle movements and stocking rate adjustments often require annual and sub-annual estimates of standing herbaceous biomass, which is influenced by plant production, livestock consumption rates, and losses of biomass to other factors such as trampling, wildlife, insects, and weather (e.g., hail). Our HLS-based models can predict standing biomass daily at 30-m spatial resolution with low error, showing current conditions as they are influenced by land management (e.g., Fig. 9) and detecting moderately low-biomass thresholds critical to adaptive management with high accuracy (74–87%). While accuracy was poor (17%) for the lowest threshold (350 kg ha^{-1}), the small sample size ($n = 6$) makes it difficult to draw conclusions on predictive performance at very low biomass values.

In terms of shortgrass rangeland management applications, decision-making for adjustment of cattle stocking rates or movement of herds to new pastures rely most on the accuracy of biomass estimates when biomass is moderately low (e.g., 350–560 kg ha^{-1}). Both our ground-based VO estimates of biomass and our remotely sensed estimates of biomass showed the greatest error when biomass was high (e.g., > 1500 kg ha^{-1}; Fig. S1 and S5), which could be due to either the rarity of this situation in our training datasets (i.e., low sample size), or spectral 'saturation'. It is well known that broadband vegetation indices using RED and NIR bands tend to be asymptotically related to vegetation biomass at high values (e.g., Sellers, 1985), though this relationship can vary with land cover and canopy structure (e.g., Baret and Guyot, 1991) and has not been thoroughly explored for indices using SWIR bands. Fortunately, in semiarid rangeland systems, time periods with high biomass are usually not a time for difficult adaptive stocking or cattle movement decisions, as forage amounts are more than sufficient. Critically, we were able to make relatively accurate predictions of when and where biomass in a grazed pasture declined to a threshold of 560 kg ha^{-1} (500 lbs. ac^{-1}), which corresponds to a level where ranchers in the shortgrass steppe may want to closely monitor cattle behavior and on-the-ground conditions to avoid forage intake limitations, declining cattle weight gains, or decreases in production potential (Bement, 1969; Porensky et al., 2021). More research is needed to understand if limitations exist for monitoring and decision-making applications specific to high-biomass situations (e.g., fire fuels mitigation, habitat modelling).

Overall accuracy of detecting when a pasture falls below a given biomass threshold could theoretically be optimized based on biomass threshold probabilities (Fig. 8), which incorporate prediction uncertainty. While rangeland managers rarely optimize for overall accuracy, the ability to estimate threshold probabilities could help to apply prediction maps to different situations. For example, a public lands manager with a mandate to avoid over-grazing may be risk averse and more willing to accept high commission error to reduce the chances of not detecting a pasture falling below a biomass threshold. In such a case, the manager could use a lower probability threshold as a decision-making trigger. Other managers may be less willing to chance moving cattle out of a pasture when sufficient forage remains, for example a rancher with limited resources for grazing or feeding cattle elsewhere. These managers may choose a higher probability threshold and accept the greater risk for omission error. Visualizing probability maps and how they are changing over time (e.g., Fig. 9) can also help to understand spatial heterogeneity associated with varying conditions related to management and environmental drivers, and to pinpoint areas in need of closer inspection or management action.

Other use-cases extend far beyond livestock management. For example, the biomass and threshold probability estimates developed in this study provide opportunities to quantify spatial patterns in wildlife habitat (e.g., nesting habitat for grassland birds; Davis et al., 2020), plan applications of prescribed fire which depend on knowledge of fine fuel loads (e.g., Augustine et al., 2014), identify locations of colonial herbivores such as prairie dogs (*Cynomys* spp.) which can dramatically affect standing biomass (e.g., Augustine and Springer, 2013 also see Fig. 9), and provide fine-scale inputs to grassland models of carbon cycling and ecosystem function (e.g., Cheng et al., 2021; Ma et al., 2019).

5. Conclusions

Process-based tools that estimate vegetation or forage production are valuable and increasingly available. However, tools for estimating standing herbaceous biomass, a key driver of adaptive management and decision-making across rangeland, grassland, and savanna ecosystems, are more limited. Our standing biomass estimation complements production-based estimates by accounting for the influence of sub-seasonal management actions (e.g., grazing rotations) and dynamic disturbance drivers (e.g., fire, burrowing mammals, hailstorms) on current vegetation conditions. In this study, we also demonstrated how we can use our model to estimate the probability that herbaceous biomass is below a given threshold, which can support more widespread adoption potential for grazing land managers with differing scenarios of risk perception and avoidance.

Our use of freely available, frequently resampled remote sensing imagery in the HLS dataset opens the door to development of near-real-time tools for standing biomass estimation, similar in concept to currently available web-based tools such as RAP (https://rangelands.app), Fuelcast (https://www.fuelcast.net), or RangeSat (https://www.rangesat.org/). By utilizing the HLS dataset, not only can we develop near-real time biomass estimates going forward, but we can also look back across the entire Landsat time series to generate historical maps

and compare current conditions to long-term averages for a given site. These near-real time and historical time series maps provide rangeland managers with an additional tool for 'learning by doing' – an integral component of adaptive management (Westgate et al., 2013) – by allowing them to monitor outcomes of management strategies across space and time. Wall-to-wall data coverage and temporally frequent resampling across huge spatial areas will help overcome many challenges associated with monitoring management outcomes in extensive rangelands, such as potential sampling biases associated with plot-based approaches and the related need to carefully stratify on-the-ground sampling efforts across space (e.g., soils and topographic features) and time (e.g., phenological phases), the latter of which may vary from season to season with the timing of precipitation. Remotely sensed biomass estimation will inherently capture even very small portions of a pasture or landscape that may have unusually high or low biomass availability (e.g., burned areas or riparian areas). These features may have outsized impacts on livestock diet quality, wildlife habitat provisioning, or other objectives, but they are difficult to account for using traditional on-the-ground biomass estimation techniques. Mapping standing biomass at fine spatial-temporal scales opens new opportunities for precision conservation, livestock, and rangeland management strategies for the sustainable provision of multiple ecosystem services from extensive rangelands.

Data availability statement

Data available through the Ag Data Commons, a digital repository hosted by National Agricultural Library.

Declaration of Competing Interest

The authors declare that they have no known competing financial interests or personal relationships that could have appeared to influence the work reported in this paper.

Acknowledgements

We sincerely thank Nick Dufek, Tamarah Jorns, Averi Reynolds, Melissa Johnston, and numerous summer students for collecting the ground-based visual obstruction (VO) and line point intercept data. Thanks to Nicole Kaplan for data management support. Funding came from the United States Department of Agriculture – Agricultural Research Service (USDA-ARS). We also thank the anonymous reviewers and Associate Editor of the journal for their service to improve the clarity, precision, accuracy, and relevance of this research manuscript. This research was a contribution from the Long-Term Agroecosystem Research (LTAR) network. LTAR is supported by the United States Department of Agriculture.

Appendix A. Supplementary data

Supplementary data to this article can be found online at https://doi.org/10.1016/j.rse.2022.112907.

References

Augustine, D.J., 2010. Spatial versus temporal variation in precipitation in a semiarid ecosystem. Landsc. Ecol. 25, 913–925. https://doi.org/10.1007/s10980-010-9469-y.

Augustine, D.J., Derner, J.D., 2015. Patch-burn grazing management, vegetation heterogeneity, and avian responses in a semi-arid grassland. J. Wildl. Manag. 79, 927–936. https://doi.org/10.1002/jwmg.909.

Augustine, D.J., Springer, T.L., 2013. Competition and facilitation between a native and a domestic herbivore: trade-offs between forage quantity and quality. Ecol. Appl. 23, 850–863. https://doi.org/10.1890/12-0890.1.

Augustine, D.J., Derner, J.D., Smith, D.P., 2014. Characteristics of burns conducted under modified prescriptions to mitigate limited fuels in a semi-arid grassland. Fire Ecol. 10, 36–47. https://doi.org/10.4996/fireecology.1002036.

Augustine, D.J., Derner, J.D., Fernández-Giménez, M.E., Porensky, L.M., Wilmer, H., Briske, D.D., 2020. Adaptive, multipaddock rotational grazing management: a ranch-scale assessment of effects on vegetation and livestock performance in semiarid rangeland. Rangel. Ecol. Manag. 73, 796–810. https://doi.org/10.1016/j.rama.2020.07.005.

Baret, F., Guyot, G., 1991. Potentials and limits of vegetation indices for LAI and APAR assessment. Remote Sens. Environ. 35, 161–173. https://doi.org/10.1016/0034-4257(91)90009-U.

Bement, R.E., 1969. A stocking-rate guide for beef production on Blue-Grama range. J. Range Manag. 22, 83. https://doi.org/10.2307/3896186.

Bolton, D.K., Gray, J.M., Melaas, E.K., Moon, M., Eklundh, L., Friedl, M.A., 2020. Continental-scale land surface phenology from harmonized Landsat 8 and Sentinel-2 imagery. Remote Sens. Environ. 240, 111685 https://doi.org/10.1016/j.rse.2020.111685.

Burnham, K.P., Anderson, D.R., 2002. Model Selection and Multi-Model Inference: A Practical Information-Theoretic Approach, 2nd ed. Springer Science & Business Media, New York, New York. https://doi.org/10.1007/b97636.

Cao, X., Chen, J., Matsushita, B., Imura, H., 2010. Developing a MODIS-based index to discriminate dead fuel from photosynthetic vegetation and soil background in the Asian steppe area. Int. J. Remote Sens. 31, 1589–1604. https://doi.org/10.1080/01431160903475274.

Chen, F., Weber, K., Gokhale, B., 2011. Herbaceous biomass estimation from SPOT 5 imagery in semiarid rangelands of Idaho. GIScience Remote Sens. 48, 195–209. https://doi.org/10.2747/1548-1603.48.2.195.

Cheng, G., Harmel, R.D., Ma, L., Derner, J.D., Augustine, D.J., Bartling, P.N.S., Fang, Q. X., Williams, J.R., Zilverberg, C.J., Boone, R.B., Hoover, D., Yu, Q., 2021. Evaluation of APEX modifications to simulate forage production for grazing management decision-support in the Western US Great Plains. Agric. Syst. 191 https://doi.org/10.1016/j.agsy.2021.103139.

Claverie, M., Ju, J., Masek, J.G., Dungan, J.L., Vermote, E.F., Roger, J.C., Skakun, S.V., Justice, C., 2018. The harmonized Landsat and Sentinel-2 surface reflectance data set. Remote Sens. Environ. 219, 145–161. https://doi.org/10.1016/j.rse.2018.09.002.

Daughtry, C.S.T., Doraiswamy, P.C., Hunt, E.R., Stern, A.J., McMurtrey, J.E., Prueger, J. H., 2006. Remote sensing of crop residue cover and soil tillage intensity. In: Handb. Environ. Chem. Vol. 5 Water Pollut, 91, pp. 101–108. https://doi.org/10.1016/j.still.2005.11.013.

Davis, K.P., Augustine, D.J., Monroe, A.P., Derner, J.D., Aldridge, C.L., 2020. Adaptive rangeland management benefits grassland birds utilizing opposing vegetation structure in the shortgrass steppe. Ecol. Appl. 30, 1–14. https://doi.org/10.1002/eap.2020.

Derner, J.D., Augustine, D.J., 2016. Adaptive management for drought on rangelands. Rangelands 38, 211–215. https://doi.org/10.1016/j.rala.2016.05.002.

Díaz-Solís, H., Grant, W.E., Kothmann, M.M., Teague, W.R., Díaz-García, J.A., 2009. Adaptive management of stocking rates to reduce effects of drought on cow-calf production systems in semi-arid rangelands. Agric. Syst. 100, 43–50. https://doi.org/10.1016/j.agsy.2008.12.007.

Edirisinghe, A., Hill, M.J., Donald, G.E., Hyder, M., 2011. Quantitative mapping of pasture biomass using satellite imagery. Int. J. Remote Sens. 32, 2699–2724. https://doi.org/10.1080/01431161003743181.

Fernández-Giménez, M.E., Augustine, D.J., Porensky, L.M., Wilmer, H., Derner, J.D., Briske, D.D., Stewart, M.O., 2019. Complexity fosters learning in collaborative adaptive management. Ecol. Soc. 24 https://doi.org/10.5751/ES-10963-240229.

Gaffney, R., Porensky, L.M., Gao, F., Irisarri, J.G., Durante, M., Derner, J.D., Augustine, D.J., 2018. Using APAR to predict aboveground plant productivity in semi-aid rangelands: spatial and temporal relationships differ. Remote Sens. 10 https://doi.org/10.3390/rs10091474.

Gaffney, R., Augustine, D.J., Kearney, S.P., Porensky, L.M., 2021. Using hyperspectral imagery to characterize rangeland vegetation composition at process-relevant scales. Remote Sens. 13 (22), 4603. https://doi.org/10.3390/rs13224603.

Gao, F., Hilker, T., Zhu, X., Anderson, M., Masek, J., Wang, P., Yang, Y., 2015. Fusing Landsat and MODIS data for vegetation monitoring. IEEE Geosci. Remote Sens. Mag. 3, 47–60. https://doi.org/10.1109/MGRS.2015.2434351.

Giam, X., Olden, J.D., 2016. Quantifying variable importance in a multimodel inference framework. Methods Ecol. Evol. 7, 388–397. https://doi.org/10.1111/2041-210X.12492.

Grigera, G., Oesterheld, M., Pacín, F., 2007. Monitoring forage production for farmers' decision making. Agric. Syst. 94, 637–648. https://doi.org/10.1016/j.agsy.2007.01.001.

Hardisky, M.A., Klemas, V., Smart, R.M., 1983. The influence of soil salinity, growth form, and leaf moisture on the spectral radiance of Spartina alterniflora canopies. Photogramm. Eng. Remote. Sens. 49, 77–83.

Hartman, M.D., Parton, W.J., Derner, J.D., Schulte, D.K., Smith, W.K., Peck, D.E., Day, K. A., Del Grosso, S.J., Lutz, S., Fuchs, B.A., Chen, M., Gao, W., 2020. Seasonal grassland productivity forecast for the U.S. Great Plains using grass-cast. Ecosphere 11. https://doi.org/10.1002/ecs2.3280.

Herrick, J.E., Van Zee, J.W., Pyke, D.A., Remmenga, M.D., Shaver, P.L., 2005. Monitoring manual Volume II : For Grassland, Shrubland and savannah Ecosystems.

Holechek, J.L., Pieper, R.D., Herbel, C.H., 1995. Range Management: Principles and Practices. Prentice-Hall.

Holling, C.S., 1978. Adaptive environmental assessment and management. In: Proc. Gulf of Mexico coastal ecosystem workshop, Sept 1979, Port Aransas Texas. John Wiley & Sons.

Holling, C.S., Meffe, G.K., 1996. Command and control and the pathology of natural resource management. Conserv. Biol. 10, 328–337. https://doi.org/10.1046/j.1523-1739.1996.10020328.x.

Irisarri, J.G.N., Derner, J.D., Porensky, L.M., Augustine, D.J., Reeves, J.L., Mueller, K.E., 2016. Grazing intensity differentially regulates ANPP response to precipitation in

North American semiarid grasslands. Ecol. Appl. 26, 1370–1380. https://doi.org/10.1890/15-1332.
Jansen, V.S., Kolden, C.A., Schmalz, H.J., 2018. The development of near real-time biomass and cover estimates for adaptive rangeland management using Landsat 7 and Landsat 8 surface reflectance products. Remote Sens. 10, 1–22. https://doi.org/10.3390/rs10071057.
Jansen, V.S., Kolden, C.A., Schmalz, H.J., Karl, J.W., Taylor, R.V., 2021. Using satellite-based vegetation data for short-term grazing monitoring to inform adaptive management. Rangel. Ecol. Manag. 76, 30–42. https://doi.org/10.1016/j.rama.2021.01.006.
Ji, L., Zhang, L., Wylie, B.K., Rover, J., 2011. On the terminology of the spectral vegetation index (NIR - SWIR)/(NIR+SWIR). Int. J. Remote Sens. 32, 6901–6909. https://doi.org/10.1080/01431161.2010.510811.
Jones, M.O., Allred, B.W., Naugle, D.E., Maestas, J.D., Donnelly, P., Metz, L.J., Karl, J., Smith, R., Bestelmeyer, B., Boyd, C., Kerby, J.D., McIver, J.D., 2018. Innovation in rangeland monitoring: annual, 30 m, plant functional type percent cover maps for U. S. rangelands, 1984–2017. Ecosphere 9. https://doi.org/10.1002/ecs2.2430.
Jones, M.O., Robinson, N.P., Naugle, D.E., Maestas, J.D., Reeves, M.C., Lankston, R.W., Allred, B.W., 2021. Annual and 16-day rangeland production estimates for the Western United States. Rangel. Ecol. Manag. 77, 112–117. https://doi.org/10.1016/j.rama.2021.04.003.
Keller, M., Schimel, D.S., Hargrove, W.W., Hoffman, F.M., 2008. A continental strategy for the national ecological observatory network. Front. Ecol. Environ. 6, 282–284. https://doi.org/10.1890/1540-9295(2008)6[282:ACSFTN]2.0.CO;2.
Lauenroth, W.K., Burke, I.C., 2008 (Eds.). Ecology of the Shortgrass Steppe: A Long-Term Perspective. Oxford University Press, New York, NY. https://doi.org/10.1093/oso/9780195135824.001.0001.
Lauenroth, W.K., Sala, O.E., 1992. Long-term forage production of North American shortgrass steppe. Ecol. Appl. 2, 397–403.
Liang, T., Yang, S., Feng, Q., Liu, B., Zhang, R., Huang, X., Xie, H., 2016. Multi-factor modeling of above-ground biomass in alpine grassland: a case study in the Three-River Headwaters Region, China. Remote Sens. Environ. 186, 164–172. https://doi.org/10.1016/j.rse.2016.08.014.
Ma, L., Derner, J.D., Harmel, R.D., Tatarko, J., Moore, A.D., Rotz, C.A., Augustine, D.J., Boone, R.B., Coughenour, M.B., Beukes, P.C., van Wijk, M.T., Bellocchi, G., Cullen, B. R., Wilmer, H., 2019. Application of grazing land models in ecosystem management: current status and next frontiers. Adv. Agron. 158, 173–215. https://doi.org/10.1016/bs.agron.2019.07.003.
Magiera, A., Feilhauer, H., Waldhardt, R., Wiesmair, M., Otte, A., 2017. Modelling biomass of mountainous grasslands by including a species composition map. Ecol. Indic. 78, 8–18. https://doi.org/10.1016/j.ecolind.2017.02.039.
Marsett, R.C.R., Qi, J., Heilman, P., Biedenbender, S.H., Watson, M.C., Amer, S., Weltz, M., Goodrich, D., Marsett, R.C.R., 2006. Remote sensing for grassland management in the arid southwest. Rangel. Ecol. Manag. 59, 530–540. https://doi.org/10.2111/05-201R.1.
Numata, I., Roberts, D.A., Chadwick, O.A., Schimel, J.P., Galvão, L.S., Soares, J.V., 2008. Evaluation of hyperspectral data for pasture estimate in the Brazilian Amazon using field and imaging spectrometers. Remote Sens. Environ. 112, 1569–1583. https://doi.org/10.1016/j.rse.2007.08.014.
Ollinger, S.V., 2011. Sources of variability in canopy reflectance and the convergent properties of plants. New Phytol. 189, 375–394. https://doi.org/10.1111/j.1469-8137.2010.03536.x.
Petersen, B., Montambault, J., Koopman, M., 2014. The potential for double-loop learning to enable landscape conservation efforts. Environ. Manag. 54, 782–794. https://doi.org/10.1007/s00267-014-0337-4.
Porensky, L.M., Derner, J.D., Augustine, D.J., Milchunas, D.G., 2017. Plant community composition after 75 yr of sustained grazing intensity treatments in shortgrass steppe. Rangel. Ecol. Manag. 70, 456–464. https://doi.org/10.1016/j.rama.2016.12.001.
Porensky, L.M., Augustine, D.J., Derner, J.D., Wilmer, H., Lipke, M.N., Fernández-Giménez, M.E., Briske, D.D., 2021. Collaborative adaptive rangeland management, multipaddock rotational grazing, and the story of the regrazed grass plant. Rangel. Ecol. Manag. 78, 127–141. https://doi.org/10.1016/j.rama.2021.06.008.
Quemada, M., Daughtry, C.S.T., 2016. Spectral indices to improve crop residue cover estimation under varying moisture conditions. Remote Sens. 8 https://doi.org/10.3390/rs8080660.
Reinermann, S., Asam, S., Kuenzer, C., 2020. Remote sensing of grassland production and management-a review. Remote Sens. 12 https://doi.org/10.3390/rs12121949.
Robel, R.J., Briggs, J.N., Dayton, A.D., Hulbert, L.C., 1970. Relationships between visual obstruction measurements and weight of grassland vegetation. Rangel. Ecol. Manag. Range Manag. Arch. 23, 295–297.
Rouse, J.W., Haas, R.H., Schell, J.A., Deering, D.W., Harlan, J.C., 1974. Monitoring the Vernal Advancement and Retrogradation (Greenwave Effect) of Natural Vegetation. College Station, Texas USA.
Safriel, U., Adeel, Z., Niemeijer, D., Puigdefabregas, J., White, R., Lal, R., Winslow, M., Ziedler, J., Prince, S., Archer, E., King, C., Shapiro, B., Wessels, K., Nielsen, T., Portnov, B., Reshef, I., Thonell, J., Lachman, E., Mcnab, D., 2005. Chapter 22: dryland systems. Ecosyst. Hum. Well-being Curr. State Trends 1, 625–664.
Sellers, P.J., 1985. Canopy reflectance, photosynthesis and transpiration. Int. J. Remote Sens. 6, 1335–1372. https://doi.org/10.1080/01431161858948283.
Smith, R.C.G., Adams, M., Gittins, S., Gherardi, S., Wood, D., Maier, S., Stovold, R., Donald, G., Khohkar, S., Allen, A., 2011. Near real-time Feed On Offer (FOO) from MODIS for early season grazing management of Mediterranean annual pastures. Int. J. Remote Sens. 32, 4445–4460. https://doi.org/10.1080/01431161.2010.487078.
Spiegal, S., Bestelmeyer, B.T., Archer, D.W., Augustine, D.J., Boughton, E.H., Boughton, R.K., Cavigelli, M.A., Clark, P.E., Derner, J.D., Duncan, E.W., Hapeman, C. J., Harmel, R.D., Heilman, P., Holly, M.A., Huggins, D.R., King, K., Kleinman, P.J.A., Liebig, M.A., Locke, M.A., McCarty, G.W., Millar, N., Mirsky, S.B., Moorman, T.B., Pierson, F.B., Rigby, J.R., Robertson, G.P., Steiner, J.L., Strickland, T.C., Swain, H. M., Wienhold, B.J., Wulfhorst, J.D., Yost, M.A., Walthall, C.L., 2018. Evaluating strategies for sustainable intensification of US agriculture through the Long-Term Agroecosystem Research network. Environ. Res. Lett. 13 https://doi.org/10.1088/1748-9326/aaa779.
Van Deventer, A.P., Ward, A.D., Gowda, P.M., Lyon, J.G., 1997. Using thematic mapper data to identify contrasting soil plains and tillage practices. Photogramm. Eng. Remote Sensing 63, 87–93.
Wehlage, D.C., Gamon, J.A., Thayer, D., Hildebrand, D.V., 2016. Interannual variability in dry mixed-grass prairie yield: a comparison of MODIS, SPOT, and field measurements. Remote Sens. 8 https://doi.org/10.3390/rs8100872.
Westgate, M.J., Likens, G.E., Lindenmayer, D.B., 2013. Adaptive management of biological systems: a review. Biol. Conserv. 158, 128–139. https://doi.org/10.1016/j.biocon.2012.08.016.
Wilmer, H., Derner, J.D., Fernández-Giménez, M.E., Briske, D.D., Augustine, D.J., Porensky, L.M., 2018. Collaborative adaptive rangeland management fosters management-science partnerships. Rangel. Ecol. Manag. 71, 646–657. https://doi.org/10.1016/j.rama.2017.07.008.
Yin, J., Wang, W., Yu, H., Liu, B., Feng, Q., Liang, T., Meng, B., Yang, S., Gao, J., Ge, J., Hou, M., Liu, J., 2020. Estimation of grassland height based on the random forest algorithm and remote sensing in the Tibetan Plateau. IEEE J. Sel. Top. Appl. Earth Obs. Remote Sens. 13, 178–186. https://doi.org/10.1109/JSTARS.2019.2954696.
Yue, J., Tian, Q., Dong, X., Xu, N., 2020. Using broadband crop residue angle index to estimate the fractional cover of vegetation, crop residue, and bare soil in cropland systems. Remote Sens. Environ. 237, 111538 https://doi.org/10.1016/j.rse.2019.111538.
Zhang, B., Zhang, L., Xie, D., Yin, X., Liu, C., Liu, G., 2016. Application of synthetic NDVI time series blended from landsat and MODIS data for grassland biomass estimation. Remote Sens. 8, 1–21. https://doi.org/10.3390/rs8010010.
Zhu, X., Helmer, E.H., 2018. An automatic method for screening clouds and cloud shadows in optical satellite image time series in cloudy regions. Remote Sens. Environ. 214, 135–153. https://doi.org/10.1016/j.rse.2018.05.024.